JCTC Journal of Chemical Theory and Computation

Nitrogen Fixation by a Molybdenum Catalyst Mimicking the Function of the Nitrogenase Enzyme: A Critical Evaluation of DFT and Solvent Effects

Alessandra Magistrato,*,† Arturo Robertazzi,† and Paolo Carloni

CNR-INFM-Democritos Modelling Center for Atomistic Simulations, International School for Advanced Studies (SISSA/ISAS) and Italian Institute of Technology (IIT) via Beirut 2-4, Trieste, Italy

Received April 23, 2007

Abstract: Compounds mimicking the enzyme nitrogenase represent promising alternative routes to the current Haber-Bosch industrial synthesis of ammonia from molecular hydrogen and nitrogen. In this work, we investigated the full catalytic cycle of one of such compounds, Mo-(HIPTN3N) (with HIPT = hexaisopropylterphenyl), by means of DFT calculations. Our results suggest these large ligands to exert mainly a steric influence on the structural properties of the catalyst. In addition, we provided a structural and electronic characterization of the putative reaction intermediates along with a picture of the electronic mechanism of molecular nitrogen N−N bond breaking. A large discrepancy was observed between calculated and experimental reaction free energies, suggesting that in the present case the predictability of DFT reaction energies is limited. Investigation of explicit solvation of specific catalytic intermediates as well as of the protonation and reducing agents reveal the crucial role played by the solvent molecules (benzene and heptane) particularly for protonation steps. Furthermore, the analysis of several DFT functionals indicates that these have to be carefully chosen in order to reproduce the energetic profile of reduction steps. This study shows how DFT calculations may be a powerful tool to describe structural and electronic properties of the intermediates of the catalytic cycle, yet, due to the complexity of the system, reaction energies cannot be easily reproduced without a careful choice of the solvation model and the exchange-correlation functional.

Introduction

Ammonia is the sixth largest chemical produced in the world.[1−4] Since the industrial synthesis from molecular nitrogen and hydrogen requires a drastic condition (500 °C at 150−200 atm),[1−4] a considerable effort is being devoted in discovering alternative routes under milder conditions of temperature and pressure.[1−4] A promising strategy is based on biomimetics (i.e., compounds that perform the same chemical reaction of natural enzymes at the same mild conditions and with no energy loss) of Fe, Mo-containing nitrogenase enzyme expressed by soil bacteria.[5−7] A major step in this direction[8−10] is the synthesis of complex **I**, in which a Mo ion is bound to a chelating triamidoamine ligand ($(RNCH_2CH_2)_3N^{3-}$) with R = hexaisopropylterphenyl or HIPT) with four nitrogen donor atoms[8−10] (Figures 1A and 2). Remarkably, the slow addition of a proton source (such as 2,6-lutidiniumBAr$_4$ where Ar is 3,5-$(CF_3)_2C_6H_3$) and a reducing agent (such as decamethylcromocene) to a solution of **I** in heptane in the presence of molecular nitrogen allows the production of ammonia with high efficiency (63−66%).[8] The proposed reaction mechanism, based on catalytic intermediates experimentally characterized,[8−11] is a Chatt-like mechanism,[8−10] in which molecular nitrogen binds the metal ion in a linear end-on-fashion (Figure 2).[11−13] However, an exhaustive understanding of this molecular processes is still lacking.[2,14]

* Corresponding author e-mail: alema@sissa.it.
† These authors equally contributed to this work.

10.1021/ct700094y CCC: $37.00
Published on Web 08/04/2007

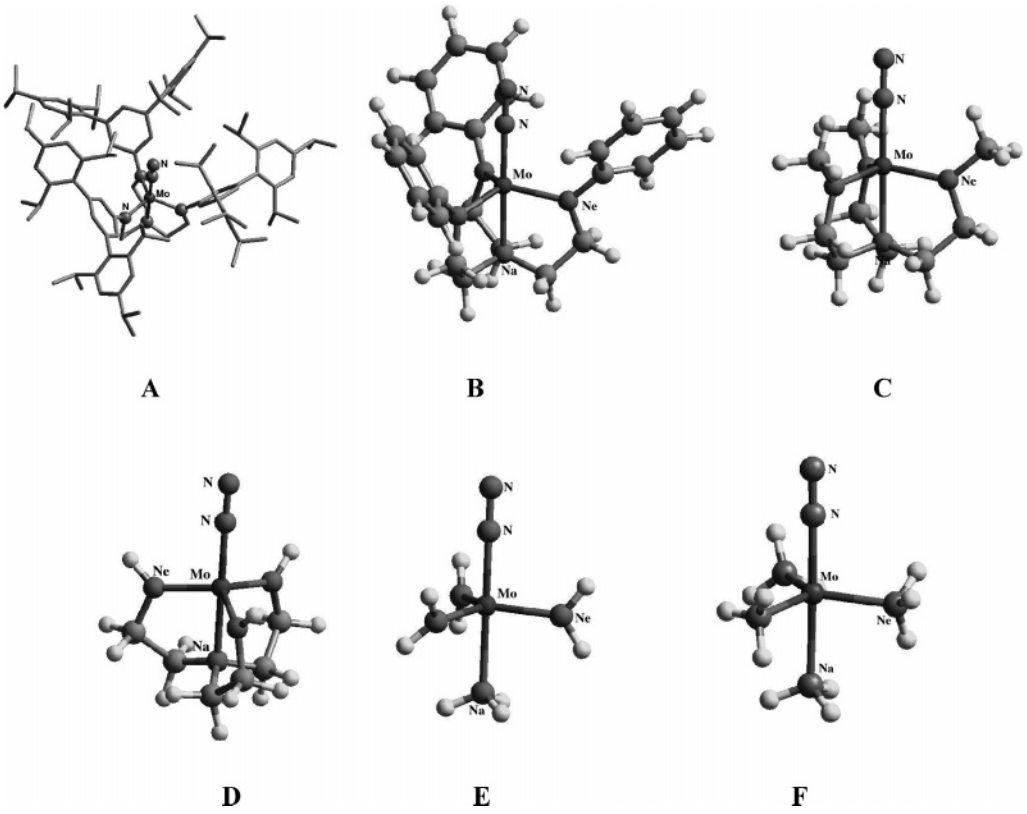

Figure 1. Computational models of **I**. **A** is the entire catalyst (hydrogen atoms are not shown for clarity). **B**−**F** are computational models of different complexity of **I**.

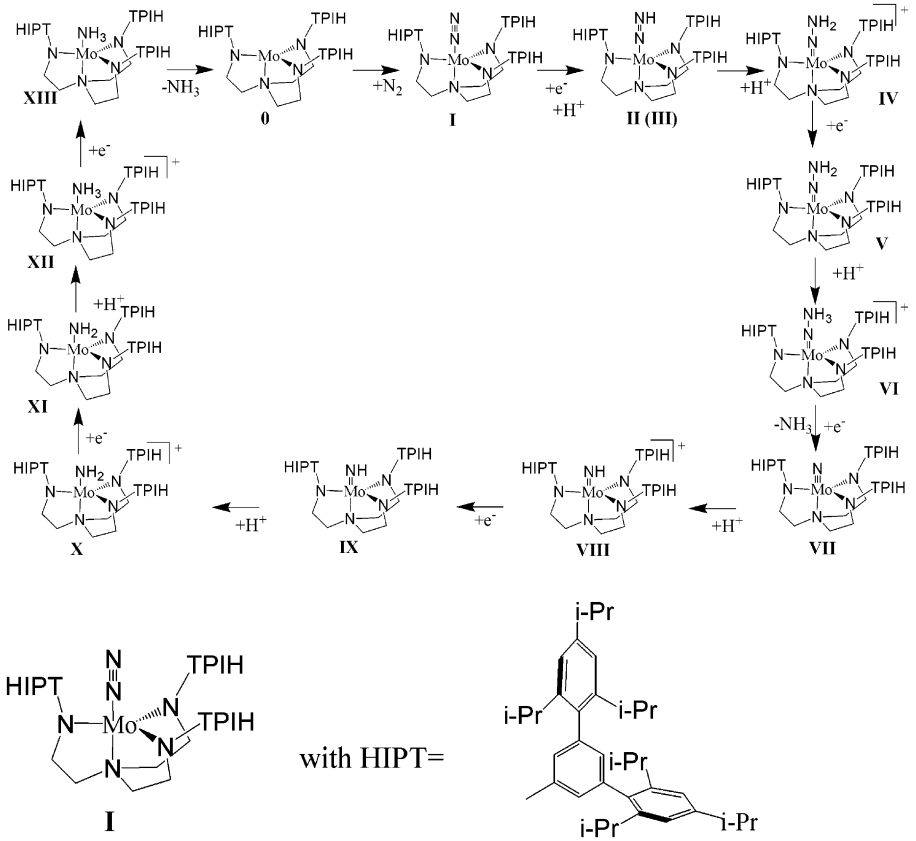

Figure 2. Schematic view of the mechanism for nitrogen fixation at a single Mo center.

In an effort to further improve the efficiency of the catalyst, the transition-metal ion has been changed,[15,16] and the R group has been modified (R = 3,5-(2,4,6-t-$Bu_3C_6H_2)_2C_6H_3$, 3,5-(2,4,6-$Me_3C_6H_2)_2C_6H_3$, 4-Br-3,5-(2,4,6-i-$Pr_3C_6H_2)_2C_6H_3$

(p-Br(HIPT)).[17] Unfortunately, none of the modified complexes has turned out to show a stronger catalytic power than that of the original compound.

Recent density functional theory (DFT) calculations with the BLYP[18,19] and B3LYP[19,20] exchange-correlation functionals, and using the PCM implicit solvation model[21] (which is widely applied to study processes involving inorganic catalysts),[22] were used to investigate the reaction mechanism.[23−26] Theoretical predictions of the catalytic intermediates and reaction energies show that geometries of molybdenum complexes are well reproduced,[25−29] while reaction energies estimated both in vacuo and with the PCM implicit solvent model turned out to be remarkably differ from the experimental free energies.[10,23,25,26] The discrepancy may be caused by several factors, including (i) the choice of the exchange-correlation functional, (ii) the absence of explicit solvation in the calculations (as solvation has been treated previously with continuum solvation models), and (iii) the lack of rigorous treatment of entropic effects.

In order to address some of these issues, we performed extensive DFT calculations on the reaction mechanism proposed in Figure 2. These include (i) static DFT calculations and (ii) dynamic (Car−Parrinello, CP)[30] DFT calculations, with PW basis sets and BP[18,31] exchange-correlation functional. Our choice for this computational method was dictated by its reliability in describing reactions catalyzed by inorganic compounds.[32,33] Subsequently, selected intermediates obtained with the latter approach were compared with DFT calculations using localized basis sets (6-31+G(d) and 6-311++G(d,p)) and B3LYP,[19,20] B3P,[20,31] PW91,[34] BHandHLYP,[19,20] and BHandH[20] exchange-correlation functionals. Calculations were carried out both in vacuo and in the presence of either an implicit solvation model (such as PCM)[18] or with a qualitative model of explicit solvation. This was obtained by including *n* solvent molecules (i.e., methane, heptane, benzene, and fluorobenzene (PhF),[35]with $1 < n < 4$).

Our calculations confirm that the nitrogen fixation promoted by **I** may proceed through a Chatt-like mechanism and that a back-donation from a filled d_{xz} Mo orbital to the empty π^*-N_2 orbital may be at the basis of the electronic mechanism responsible for the N_2 cleavage. However, in line with previous DFT studies, our calculations reveal large discrepancies between experimental free energies and calculated reaction energies.[10,23,25] Such evident failures may be prevented by explicitly accounting for solvent effects (even for apolar solvents) for the protonation steps, whereas a careful choice of the DFT exchange-correlation functional is required for reductions steps.[36] Thus, this work reveals DFT potentialities and limitations, suggesting that the predictive abilities of DFT techniques may be limited for this intricate catalytic system and that solvent effects (typically neglected) may play a significant role.

Computational Details

Several models of the catalyst of different complexity were taken into account, i.e., from the entire catalyst (**A**) to the molybdenum complexes containing triphenylamidoamine, trimethylamidoamine, triamidoamine, amide, and ammonia ligands (**B**−**F**, respectively in Figure 1).

DFT calculations were initially performed with the Amsterdam Density Functional program ADF2000.01.[37,38]A spin unrestricted formalism was applied to open shell systems, and structures of each catalytic intermediate were optimized for all possible spin states. Calculations were performed with the gradient-corrected model developed by Becke (B),[18] combined with the Perdew's correlation term (P).[31] The electronic configurations of molecular systems were described by a triple-STO basis set on the Mo center for the ns, np, nd, (n+1)s, and (n+1)p valence shells; a double-STO basis set was used for C (2s 2p), N (2s, 2p), and H(1s). Inner shells of the atoms were treated within the frozen core approximation. ZORA[39] relativistic corrections were added to the total energy of Mo.

Static and dynamic density functional calculations were performed with Car−Parrinello molecular dynamics simulations.[30] These simulations combine a classical molecular dynamics scheme with an electronic structure calculation in the framework of density functional theory (DFT), a pseudopotential formalism, periodic boundary conditions, and a basis set of plane waves (PW). Calculations reported in this work were performed with the program CPMD.[40] In this study, we employed analytical pseudopotentials for Mo and Cr of the Goedecker type[41] and nonlocal, norm conserving pseudopotentials of the Martins−Trouiller type[42] for all the other elements except for H. For these an analytical local pseudopotential was used. Moreover, 14 valence electrons and a reference configuration of $4s^2 4p^6 4d^5 5s^1$ and $3s^2 3p^6 3d^5 4s^1$ were considered for Mo and Cr, respectively. Pseudopotentials for N and C were transformed to a fully nonlocal form by adopting the scheme developed by Kleinman and Bylander.[43] A kinetic energy cutoff of 70 Ry was applied to all the calculations. In order to properly describe charged systems, periodic images were decoupled using the scheme of Hockney.[44] A face centered cubic (FCC) super cell of the edge of 25 Å was employed for **A**. In addition, a simple cubic (SC) cell of edge $a = 16$ Å was used for all other calculations. Classical equations of motion were integrated with a velocity Verlet algorithm with a time step of 0.145 fs and a fictitious mass for the electronic degrees of freedom of $\mu = 800$ au. Geometry optimization runs were also carried out within the CPMD code.[40] These calculations were performed with a preconditioned conjugate gradient procedure.[40] All the calculations were performed within a spin unrestricted formalism.

Calculations on selected reaction intermediates (**III**, **IV**, **V**, **VII**, **VIII**, and **IX**, Figure 2), the proton source, and the reductant were also carried out using the Gaussian03 suite of programs[45] in vacuo and in the presence of implicit and explicit solvent.

6-31+G(d) and 6-311++G(d,p) basis sets were employed with the B3LYP,[19,20] B3P,[18,31] PW91,[34] BHandHLYP,[19,20] and BHandH[20] exchange-correlation functionals. In order to evaluate the effect of implicit solvent molecules, the polarized continuum model, PCM, was employed.[21,22] In addition, calculations were carried out in the presence of *n* solvent molecules (i.e., methane, heptane, benzene, and fluoroben-

zene (PhF),[35] with $1 < n < 4$). We are aware that such a static first solvation shell is only a rough representation of solvation, which is a very complex dynamical phenomenon. Due to the size of the solute/solvent adducts, geometries were fully optimized with a reduced threshold, which sets the optimization convergence criteria to a maximum step size of 0.01 au and an rms force of 0.0017 au.

Energetics for Each Reaction Step. Reaction energies were calculated for each step of the catalytic cycle as reported below. We would like to remark that no entropic effects have been considered.

(i) Reaction energy of protonation ($\Delta E_{R,prot}$): $\Delta E_{R,prot} = E_{product} + E_{Lut} - E_{reactant} - E_{LutH+}$, where $E_{product}$ and $E_{reactant}$ are the energies of the protonated and neutral catalyst, respectively; E_{Lut} and E_{LutH+} are the energies of the protonation agent (lutidinium, Lut), in the unprotonated and protonated state, respectively.[8−10]

(ii) Reaction energy of reduction ($\Delta E_{R,red}$): $\Delta E_{R,red} = E_{product} + E_{dmCr^+} - E_{reactant} - E_{dmCr}$, where $E_{product}$ and $E_{reactant}$ are the energies of the catalyst in the reduced and oxidized form, respectively; E_{dmCr^+} and E_{dmCr} are the energies of the reducing agent (decamethylcromocene, dmCr) in the oxidized and reduced state, respectively.

Solvent effects and exchange-correlation influence were considered for the calculated reaction energies of the fourth, fifth, eighth, and ninth steps of the catalytic cycle for which experimental free energies are available.[10] Steps leading to the formation of an intermediate (i.e., **I**) were labeled as Sn, with n equal to the number of the intermediate (i.e., **SI**).

(iii) Reaction energies were estimated with an implicit solvent ($\Delta E_R{}^S{}_{PCM}$). Thus, reaction energies in an implicit solution were calculated as follows: $\Delta E_R{}^S{}_{PCM} = E^S{}_{PCM}$(product) + $E^S{}_{PCM}$(LutH$^+$ or dmCr$^+$) − $E^S{}_{PCM}$(reagent) − $E^S{}_{PCM}$(Lut or dmCr). Solvation energies were also estimated with an explicit solvent ($\Delta E^S{}_{exp}$) as $\Delta E^S{}_{exp} = E_{solute/solvent} - E_{solute} - nE_{solvent}$, where $E_{solute/solvent}$ is the energy of the solute in the presence of n ($1 < n < 4$) solvent molecules, E_{solute} is the energy of the solute in vacuo, and $E_{solvent}$ is the energy of each single solvent molecule. Since solvation is shown to have a larger impact on relative energies of Lut/LutH$^+$ and dmCr/dmCr$^+$ and to a minor extent on relative energies on reaction intermediates (vide infra), explicit solvation effects on reaction intermediates were neglected. Thus, reaction energy upon explicit solvation was given by $\Delta E_R{}^S{}_{exp}$ = E(product) + $E^S{}_{exp}$(LutH$^+$ or dmCr$^+$) − E(reagent) − $E^S{}_{exp}$(LutH or dmCr). Errors with respect to experimental free energies (ΔG_{mes})[10] are given as $\Delta\Delta E_R$, $\Delta\Delta E_R{}^S{}_{PCM}$, and $\Delta\Delta E_R{}^S{}_{exp}$ where $\Delta\Delta E_R = |\Delta E_R - \Delta G_{mes}|$, $\Delta\Delta E_R{}^S{}_{PCM} = |\Delta E_R{}^S{}_{PCM} - \Delta G_{mes}|$, and $\Delta\Delta E_R{}^S{}_{exp} = |\Delta E_R{}^S{}_{exp} - \Delta G_{mes}|$.

Calculated Properties. Bond orders and Boys orbitals were calculated for all the complexes studied in this work.[46,47] Based on Boys orbitals, the bond ionicity BI_{AB} was calculated as in ref 48, namely $BI_{AB} = (d_A)/(d_{AB})$, where d_A is the distance between atom A and the Boys orbital along the AB bond; d_{AB} is the length of the bond between A and B. The analysis of BI_s is a useful tool to individuate lone pairs and provides an estimation of the ionicity of chemical bonds.[48]

To analyze intermolecular solute/solvent interactions, the Atoms In Molecules (AIM) theory was employed.[49,50] Topological analysis of computed electron densities (ρ) was performed using the AIM2000 package.[51] AIM is based upon those critical points (CPs) where the gradient of the density, $\nabla\rho$, vanishes. Such points are classified by the curvature of the electron density, for example bond critical points (BCPs) have one positive curvature (in the internuclear direction) and two negative (perpendicular to the bond). Properties evaluated at such BCPs characterize the bonding interactions present[52] and have been widely used to study intermolecular interactions. Recently, the AIM based method has been applied for quantifying π-stacking interactions.[53]

Results

1. Structural and Electronic Properties of I. Structural parameters of **I** (**A**, in Figure 1), calculated with PW basis set and BP[18,31] gradient corrections, compare well with those of the X-ray structure.[9,10] In particular, all bond lengths range within $\Delta d \sim 0.03$ Å, except the N_1-N_2 and $Mo-N_a$ bond distances, for which differences are of $\Delta d \sim 0.09$ Å and ~0.06 Å, respectively. However, the estimated N_1-N_2 bond length is in line with previous theoretical calculations.[23,25,28,54] Furthermore, test calculations performed for an isolated N_2 molecule give a N_1-N_2 distance in excellent agreement with the experimental value ($N_1-N_2 = 1.11$ Å and 1.0975 Å,[11] respectively) suggesting that our computational setup is reliable for the dinitrogen moiety. Thus, the error observed in the N_1-N_2 distance of **A** may be partly due to our theoretical description and partly caused by strong N_2 thermal motions which may render the experimental N_1-N_2 distance mistakenly shorter.[8−10]

In contrast, discrepancies observed for $Mo-N_a$ may be ascribed to the chelating triamidoamine ligand backbone rigidity, i.e., the small error of calculated CH_2-CH_2 and CH_2-N_a bonds ($\Delta d = +0.01$ Å and $\Delta d = +0.02$ Å compared to the X-ray structure, respectively) may force the $Mo-N_a$ bond to elongate in order to avoid angular strain.

2. Choice of the Model System. Our calculations on **A** reproduce fairly well the experimentally available structural properties of **I**. However, calculations of the reaction energies of the entire catalytic cycle (Figure 2) as well as the estimation of solvation effects employing model **A** are not feasible due to the large size of the system. We attempted to identify a more computationally suitable model which retains the most relevant chemical features of **I** by comparing the main structural and electronic properties of **A** with those of simpler models, from **B** to **F**. In these models the hexaisopropylterphenyl aminoamine ligand was replaced by triphenylaminoamine (**B**), trimethylaminoamine (**C**), triamidoamine (**D**), by tree amine and one ammonia ligands (**E**), and finally by four ammonia ligands (**F**) (Figure 1). The accuracy of using model **B** for our calculations was tested performing calculations with PW, STO, and Gaussian basis sets with BP[18,31] (see Table S1, in the Supporting Information). These confirm a negligible dependence of the structural properties on the basis set used. Notably, the agreement between **A** and **B** is excellent ($\Delta d = +0.01$ Å with respect to **A**, Table 1). Furthermore, the HOMO orbital of **B** is characterized by a back-bonding from the occupied d_{xz} of

Table 1. Selected Experimental and Calculated Bond Lengths of **A** and **B** (Figure 1)

bond (Å)	X-ray [9,10]	**A**	**B**
$Mo-N_1$	1.96	1.98	1.99
N_1-N_2	1.06	1.15	1.15
$Mo-N_a$	2.19	2.24	2.25
$Mo-N_e$	1.98	2.01	2.00
$N_e-C(Ph)$	1.45	1.42	1.41
N_e-CH_2	1.47	1.47	1.48
CH_2-CH_2	1.51	1.52	1.53
CH_2-N_a	1.47	1.49	1.50

Mo to the empty π^* orbital of the nitrogen molecule (Figure S2a).[54]

Comparison of the structural parameters of **A** and **B** suggests the coordination sphere of **I** to be hardly affected by HIPTs. This may be consistent with experimental findings of HIPTs avoiding the formation of catalyst dimers.[2,8−10] Thus, our calculations confirm the experimental hypothesis that the structural properties of the catalyst are mainly dictated by the rigid geometry of the chelating triamidoamine ligand,[2,8−10] the HIPT substituents playing only a steric role.[2,8]

From a comparison of structural and electronic properties of models **B**−**F** (Supporting Information, Table S2), we conclude that **B** represents a good tradeoff between accuracy and computational cost to explore the entire energetic profile of dinitrogen reduction at a single Mo center. Therefore, model **B** was employed for all calculations reported in this work.

3. The Catalytic Mechanism. A detailed electronic and structural analysis of possible catalytic intermediates was carried out using **B** as model of **I**. Typically, reaction intermediates are more stable in the low spin state than in the higher spin state with the only exception of **XII**, for which the triplet state is the most likely.

Albeit not observed experimentally,[2,8−10] the isolated Mo complex (**0** in Figure 2) turns out to be a stable intermediate. Comparison with **I** shows that the absence of N_2 causes a decrease of the $Mo-N_a$ axial bond by $\Delta d = -0.11$ Å accompanied by a bond order (BO) increase, $\Delta BO = +0.1$ (Tables 2 and 3, respectively). Notably, the analysis of the Kohn−Sham orbitals supports experimental hypotheses that the $Mo-N_a$ weakening upon N_2 coordination may be caused by the *trans* influence of the N_2 ligand itself (Figure S2b).[55]

Formation of **I** starting from N_2 and **0** is exergonic ($\Delta E \sim -29$ kcal/mol) (Figure 3).[56] The bond order[46] of coordinated N_2 (BO = 2.3) is significantly smaller with respect to that of free nitrogen (BO = 3.0). This may be caused by the back-bonding from the occupied d_{xz} of the metal ion to the empty π^* orbital of the nitrogen molecule, as described by the HOMO orbital (Figure S2a). This strengthens the $Mo-N_1$ bond, in turn weakening the N_1-N_2 bond. Furthermore, the lone pair localized on N_1, identified by its Boys orbital,[47,48] is polarized upon the formation of the $Mo-N_1$ bond (Figure S5a), and it can no longer be exclusively attributed to N_1 ($BI_{MoN} = 0.78$) (Table 4.). Notably, a triple covalent bond is present between the two nitrogens as the bond ionicity indexes (which provide a picture of the polarity of chemical bonds) are close to 0.5 (BI_{N1-N2} of 0.40, 0.48, 0.49) (Figure S5a).[48] However, one bond is slightly polarized, in agreement with a N_1-N_2 bond order lower than three.

According to experimental suggestions,[8−10] the next step of the cycle involves the simultaneous protonation and reduction of the catalyst with formation of a diazenido complex. However, formation of a positively charged diazenido complex has not been completely ruled out.[2,8−10] Yet, this intermediate has been characterized by previous theoretical calculations,[25,28] and the existence of similar intermediates has been shown for different catalysts.[12] Indeed, we do find a stable positively charged diazenido (**II**) species (Figure 2), but the protonation process **SII** is endoergonic (Figure 3). The N_1-N_2 bond length increases ($\Delta d = +0.08$ Å), and in turn its bond order decreases ($\Delta BO = -0.5$) compared to **I**, N_1-N_2 becoming only double ($BI_{N1N2} = 0.57, 0.58$). Hybridization changes of both N_2 nitrogen atoms cause a bending of $Mo-N_1-N_2$ by a few degrees (Table 2). The $Mo-N_1$ distance decreases by $\Delta d = -0.14$ Å, and it is associated to an increase of bond order ($\Delta BO = +0.5$) with the formation of a metal−nitrogen double bond ($BI_{MoN} = 0.65, 0.65$).

Subsequent reduction, with formation of a neutral diazenido complex (**III**), is exergonic (Figure 3). Comparison with **II** shows that reduction weakens N_1-N_2 ($\Delta d = +0.02$ Å, $\Delta BO = -0.2$) but strengthens $Mo-N_1$ ($\Delta d = -0.04$, $\Delta BO = +0.2$). The reaction proceeds with a further protonation and subsequent formation of a positively charged hydrazido intermediate (**IV**), with $Mo-N_1$ being stronger than that of **III** ($\Delta d = -0.04$ Å, $\Delta BO = +0.2$). Indeed the BO analysis reveals that $Mo-N_1$ is triple with a slight ionic degree in **IV** ($BI_{Mo-N1} = 0.66, 0.65, 0.68$). A further weakening of the N_1-N_2 bond ($\Delta d = +0.07$ Å, $\Delta BO = -0.3$) occurs, showing an ionic and a covalent bond ($BI_{N1N2} = 0.84, 0.52$). A lengthening of the $Mo-N_a$ bond parallels these structural transformations ($\Delta d = +0.04$ Å, $\Delta BO = -0.1$), while the $Mo-N_1-N_2$ angle bends to 171°. Unlike **SII**, **SIV** is exergonic (Figure 3). Remarkably, comparison of calculated ΔE[36] and experimental reaction free energies of **SIV** shows a large discrepancy ($\Delta\Delta E_R \sim 17$ kcal/mol). Previous theoretical calculations (carried out with different models of the catalyst and solvated with an implicit solvent model)[21] showed a slightly smaller and yet significant error ($\Delta\Delta E_R{}^S{}_{PCM} \sim 10$ kcal/mol).[25] Possible sources of error for this large discrepancy are addressed below (vide infra). **SV** leads to reduction of **IV** to a neutral hydrazido complex (**V**), the process being exergonic (Figure 3). In contrast to the observed trend, reduction weakens the $Mo-N_1$ bond ($\Delta d = +0.06$, $\Delta BO = -0.3$), while it hardly affects N_1-N_2. BI_{N1N2} values indicate that a covalent (0.42) bond and an ionic (0.84) bond are present. As the $Mo-N_1-N_2$ angle further bends to 159°, one of the electron pairs forming the triple $Mo-N_1$ bond gains a stronger ionic character ($BI_{Mo-N1} = 0.88$), while the other ones show a double covalent character (0.65, 0.60). As for **SIV**, a large discrepancy is observed between calculated and experimental reaction energies of **SV** ($\Delta\Delta E_R \sim 9$ kcal/mol). Yet, the error is sensibly smaller than that of the previous protonation step. As seen for **SIV**, inclusion of an implicit solvent model improves the agreement, $\Delta\Delta E_R{}^S{}_{PCM} \sim 3$ kcal/mol.[25]

Table 2. Selected Bond Lengths (Å) and Angles (deg) of Each Catalytic Intermediate

	Mo **0**	MoN_2 **I**	$MoNNH^+$ **II**	MoNNH **III**	$MoNNH_2^+$ **IV**	$MoNNH_2$ **V**	$MoNNH_3^+$ **VI**
$Mo-N_1$		1.99	1.85	1.81	1.77	1.83	1.84
N_1-N_2		1.14	1.22	1.24	1.31	1.31	1.51
$Mo-N_{e1}$	2.02	2.02	2.00	2.00	2.00	2.04	1.98
$Mo-N_{e2}$	2.01	2.03	2.01	2.02	2.01	2.05	2.02
$Mo-N_{e3}$	2.02	2.02	1.99	2.01	2.02	2.03	2.02
$Mo-N_a$	2.14	2.25	2.30	2.28	2.32	2.31	2.37
$Mo-N_1-N_2$		180	177	176	171	159	131
	MoN **VII**	$MoNH^+$ **VIII**	MoNH **IX**	$MoNH_2^+$ **X**	$MoNH_2$ **XI**	$MoNH_3^+$ **XII**	$MoNH_3$ **XIII**
$Mo-N_1$	1.68	1.74	1.75	1.93	1.94	2.22	2.30
$Mo-N_{e1}$	2.04	1.99	2.05	1.99	2.02	1.99	2.02
$Mo-N_{e2}$	2.03	2.00	2.04	2.00	2.01	2.01	2.03
$Mo-N_{e3}$	2.04	2.00	2.09	1.99	2.03	1.99	2.04
$Mo-N_a$	2.45	2.37	2.37	2.34	2.30	2.25	2.20

Table 3. Selected Bond Orders[46] for Characteristic Bond Lengths of Each Catalytic Intermediate

bond order	Mo **0**	MoN_2 **I**	$MoNNH^+$ **II**	MoNNH **III**	$MoNNH_2^+$ **IV**	$MoNNH_2$ **V**	$MoNNH_3^+$ **VI**
$Mo-N_1$		0.5	1.0	1.2	1.3	1.0	1.1
N_1-N_2		2.3	1.7	1.5	1.2	1.2	0.8
$Mo-N_{e1}$	0.5	0.5	0.6	0.5	0.6	0.5	0.5
$Mo-N_{e2}$	0.5	0.5	0.6	0.5	0.6	0.5	0.6
$Mo-N_{e3}$	0.5	0.5	0.6	0.5	0.6	0.5	0.5
$Mo-N_a$	0.3	0.2	0.2	0.1	0.2	0.1	0.1
bond order	MoN **VII**	$MoNH^+$ **VIII**	MoNH **IX**	$MoNH_2^+$ **X**	$MoNH_2$ **XI**	$MoNH_3^+$ **XII**	$MoNH_3$ **XIII**
$Mo-N_1$	2.1	1.5	1.5	0.7	0.7	0.1	0.1
$Mo-N_{e1}$	0.5	0.6	0.6	0.6	0.5	0.5	0.5
$Mo-N_{e2}$	0.5	0.6	0.6	0.6	0.5	0.6	0.5
$Mo-N_{e3}$	0.5	0.6	0.6	0.6	0.5	0.5	0.5
$Mo-N_a$	0.1	0.1	0.1	0.1	0.1	0.2	0.2

Upon protonation of **V**, formation of a positively charged hydrazidium complex (**VI**) is exergonic (Figure 3). The additional proton leads to a further weakening of $Mo-N_1$ and N_1-N_2 bonds, $\Delta d = +0.01$ Å, $\Delta BO = -0.1$ and $\Delta d = +0.2$ Å, $\Delta BO = -0.4$, respectively. As a result (i) no electron pairs are present along the N_1-N_2 bond, while one pair is localized on N_2 ($BI_{N1N2} \sim 1$); (ii) the $Mo-N_1$ bond exhibits a double bond character ($BI_{MoN1} = 0.68, 0.69$); and (iii) the $Mo-N_1-N_2$ angle bends up to 131°.

SVII involves reduction of **VI** with the formation of a nitrido complex and the release of NH_3. The stability of a neutral hydrazidium complex was tested by adding one electron to **VI**. In line with the experiments, release of ammonia spontaneously occurs during DFT-based molecular dynamics simulations on the reduced form of **VI** at 0 K, suggesting that no energy barrier is expected for the formation of **VII**. Moreover, reduction is very exergonic (Figure 3). Interestingly, **VII** is characterized by a strengthening of $Mo-N_1$ ($\Delta d = -0.16$ Å, $\Delta BO = +1.0$), which gains the character of a triple bond ($BI_{Mo-N1} = 0.57, 0.57, 0.50$) (Figure S5b), along with a further weakening of $Mo-N_a$ ($\Delta d = +0.08$ Å, $\Delta BO = -0.5$).

The further stepwise protonation and reduction leads to formation of a positively charged and a neutral imido intermediate (**VIII** and **IX**). In both complexes, $Mo-N_1$ is weaker ($\Delta d = +0.07$ Å, $\Delta BO = -0.6$) with a strong ionic character ($BI_{Mo-N1} = 0.68, 0.68, 0.66$), compared to that of **VII**. The $Mo-N_e$ bond is stronger in **VIII** (average value $\Delta d = -0.04$ Å, $\Delta BO = 0.0$) than in **IX**. Moreover, protonation is exergonic, while reduction is endoergonic (Figure 3). Unfortunately, despite the satisfactory agreement between calculated and experimental structures of the intermediates,[9,10] estimated reaction energies differ remarkably from measured ones ($\Delta\Delta E_R \sim 16$ and $\Delta\Delta E_R \sim 10$ kcal/mol, for **SVIII** and **SIX**, respectively). As for **SIII** and **SIV**, inclusion of an implicit solvent model slightly improves the agreement ($\Delta\Delta E_R{}^S{}_{PCM} \sim 12$ and $\Delta\Delta E_R{}^S{}_{PCM} \sim 6$ kcal/mol, for **SVIII** and **SIX**, respectively).[25]

The cycle proceeds with the formation of a positively charged and a neutral amido intermediates (**X** and **XI**, respectively). These exhibit a significant weakening of the $Mo-N_1$ bonds ($\Delta d = +0.19$ Å, $\Delta BO = -0.8$). However, a difference of $\Delta d \sim 0.06$ Å ($\Delta BO \sim -0.8$) is observed in the $Mo-N_e$ bonds, of **X** and **XI**, with **X** showing the

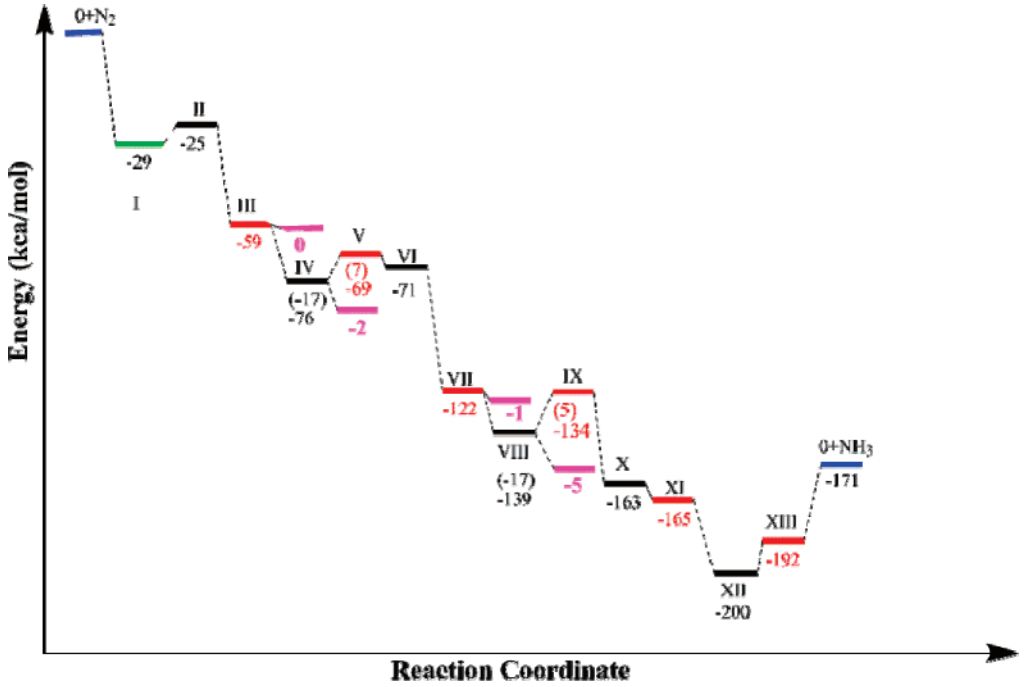

Figure 3. Reaction energy profiles. The green line represents the binding energy of N_2 to the catalyst. The black lines represent protonation steps. Red lines are reduction steps. The blue line represents the release of NH_3. Magenta lines refer to experimental ΔG.[10] Reaction energies are given with respect to 0 intermediate. For those steps for which experimental reaction energies are available we report calculated reaction energies and experimental free energies relative to the preceding intermediate in parentheses.

Table 4. Bond Ionicity for Mo−N_1 and N_1−N_2 Bonds for Each Catalytic Intermediate[a]

BI_{AB}	MoN_2 **I**	$MoNNH^+$ **II**	MoNNH **III**	$MoNNH_2^+$ **IV**	$MoNNH_2$ **V**	$MoNNH_3^+$ **VI**
Mo−N_1	0.78	0.65	0.65	0.66	0.88	0.96
Mo−N_1		0.65	0.63	0.65	0.62	0.69
Mo−N_1				0.60	0.61	0.68
N_1−N_2	0.40	0.58	0.56	0.84	0.84	1
N_1−N_2	0.48	0.57	0.55	0.51	0.42	
N_1−N_2	0.49					

BI_{AB}	MoN **VII**	$MoNH^+$ **VIII**	MoNH **IX**	$MoNH_2^+$ **X**	$MoNH_2$ **XI**	$MoNH_3^+$ **XII**	$MoNH_3$ **XIII**
Mo−N_1	0.57	0.68	0.73	0.78	0.78	0.77	0.79
Mo−N_1	0.57	0.68	0.73	0.71	0.71		
Mo−N_1	0.56	0.66	0.65				

[a] BI_{AB} is defined as $BI_{AB} = (d_A)/(d_{AB})$ where d is the displacement of the Boys orbitals along the bond and A = Mo and N_1 and B = N_1 and N_2, for Mo−N_1 and N_1−N_2 bonds, respectively.[47,48]

strongest ones. Furthermore, **SX** is exergonic, while **SXI** is endoergonic (Figure 3). Formation of the amido complex provokes a rearrangement of the charge density to accommodate the additional proton. This implies a double polarized Mo−N_1 bonds ($BI_{Mo-N1} \sim 0.78, 0.71$) in both the charged and the neutral compounds.

A final protonation leads to formation of a positively charged ammine intermediate (**XII**), in which the Mo−N_1 bond is weaker ($\Delta d = +0.28$ Å, $\Delta BO = -0.5$) with a single polar Mo−N_1 bond ($BI_{Mo-N1} = 0.77$).

The final reduction step determines the formation of a neutral ammine intermediate (**XIII**), which is characterized by an even weaker Mo−N_a bond ($\Delta d = +0.08$) with respect to **XII** and by a single Mo−N_1 ionic ($BI_{MoN1} = 0.79$) bond character. **SXII** is exergonic, and formation of **XIII** proceeds with no gain in reaction energy.

At the end of the cycle, a second NH_3 is released. The process is endoergonic by 21 kcal/mol (Figure 3).[56] This suggests that the activation energy of the process must be larger than this relatively high value, indicating that dissociation of the second ammonia molecule may be a slow step of the catalytic cycle. Indeed, the exchange between NH_3 and N_2 is exergonic by $\Delta E_{exc} = -8$ kcal/mol. However, it is not clear whether the reaction proceeds through an associative or a dissociative mechanism.[14]

Discussion

General Structural and Electronic Features of the Catalytic Cycle. Our calculations confirm experimental hypoth-

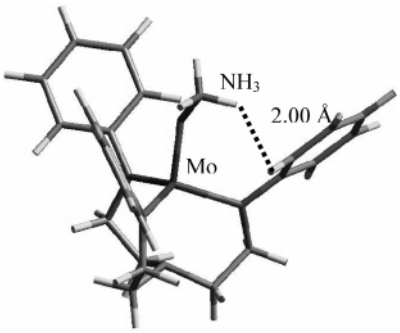

Figure 4. $MoNNH_3^+$ intermediate (**VI**). Steric contacts between a hydrogen of the NNH_3 ligand and the phenyls substituents are shown.

eses that the presence of a bulky substituent such as HIPT imposes the end-on-fashion coordination of N_2 and in turn allows for an efficient back-donation.[2,8]

In addition, our results suggest that the molecular nitrogen activation performed by the Mo catalyst is mainly caused by a back-bonding from the filled Mo d_{xz} orbital to the empty π^*-$N_1-N_2H_n$ (with $n = 0-2$) orbital, which is ubiquitous in the reaction intermediates **I**−**V** (Figure S2a). The transfer of electron density from the metal center to the π^*-$N_1-N_2H_n$ orbital strengthens Mo−N_1 and weakens the dinitrogen bond, leading to its cleavage.

The Mo−N_1 bond length does not decrease monotonically in the first half of the catalytic cycle. This may be ascribed to two factors: (i) the bending of the Mo−N_1-N_2 angle (initially collinear) causes the newly formed NH_3 group to experience steric repulsion from the phenyl group (minimum distance as short as 2.0 Å, Figure 4)[57] and the steric repulsion hampers the shortening of the Mo−N_1 bond and (ii) the back-bonding from the occupied d_{xz} metal orbital to the π^*-N_2-orbital becomes progressively less effective as the triple and double dinitrogen bonds are broken. This may also hamper the strengthening of the Mo−N_1 bond.

Experimental vs Calculated Reaction Energies of SIV, SV, SVIII, and SIX

Solvation Effects on Protonation Steps. As shown in Figure 3 the exergonic character of the protonation steps **SIV** and **SVII** for which experimental measurements are available is largely overestimated by DFT calculations ($\Delta\Delta E_R = 17$, 16 kcal/mol, respectively).[10] In order to explore possible sources of such discrepancy, DFT calculations with BP,[18,31] B3LYP,[19,20] and BHandH[20] exchange-correlation functionals have been performed on both the catalyst (model **B)** and the proton source.

In line with previous findings,[24−28] our in vacuo calculations confirm that geometries of molybdenum complexes and reaction energies of protonation steps do not depend significantly on the exchange-correlation functional used, Tables 5, S2, and S3. However, **SIV** and **SVIII** reaction energies do differ from experimental free energies, Table 5.[25] Taking into account solvent effects with an implicit solvent model,[21] as in previous studies,[25,26] only slightly reduces the discrepancy to $\Delta\Delta E_R{}^S{}_{PCM} \sim 10$ and ~ 12 kcal/mol, for **SIV** and **SVIII**, respectively.[25] This error is well beyond that typical of DFT calculations and confirms that other factors may be at the basis of such a discrepancy.[58]

Since reaction energies are rather independent of the exchange-correlation functional used,[24−27] and PCM[21] only slightly improves the agreement, the observed error may be due to a lack of explicit description of solvent effects. Albeit experimental studies demonstrated that the solubility of the reactive species is limited in heptane solution,[2,59] the aromatic rings of both molybdenum species and proton source suggest the presence of solute/solvent hydrophobic interactions. Thus, we explored the effect of an increasing number of explicit solvent molecules (from one methane molecule up to four heptane and benzene molecules) on the energetics of **SIV** and **SVIII**. Since solute/solvent interactions should mainly be C−H...π and π...π, the use of the most popular DFT functionals is not appropriate.[60] In contrast, correlated ab initio methods (such as MP2[61] and CCSD),[62] which account for dispersion interactions, are computationally too demanding for such systems. A valuable alternative is constituted by the DFT-BHandH[20] as it has recently been shown to describe dispersion interactions with the similar accuracy of CCSD[62] calculations but at an affordable computational cost.[63] Indeed, the BHandH functional[20] has been successfully applied to a variety of systems governed by dispersion forces, showing excellent results.[63,64] Interestingly, preliminary data (not reported) indicate that interaction energies of a prototypical example of a C−H...π bonded system (CH_4...benzene) obtained with BHandH/6-31+G(d) are in good agreement with those estimated with high level calculations.[65] Moreover, test calculations reported in the Supporting Information confirm the reliability of the BHandH[20]/6-31+G(d) calculations to reproduce the geometries of the molybdenum complexes (Tables S2−S4). Thus, we fully optimize solutes (reaction intermediates as well as $LutH^+$ and Lut) in the presence of explicit solvent molecules (Figure 5 and Table 6).

A first test to estimate the impact of C−H...π interactions was carried out with methane. The interaction of catalytic intermediates with a methane molecule turns out to similarly stabilize molybdenum complexes involved in **SIV** and **SVIII** as the difference in solvation energies, $\Delta\Delta E_{exp\ (MoN/MoNH+)}$ and $\Delta\Delta E^S{}_{exp\ (MoNNH/MoNNH2+)}$, is less than 0.5 kcal/mol, Table 6. In contrast, Lut and $LutH^+$ solvation energies differ by $\sim$3 kcal/mol as the former gains $\sim$2 kcal/mol upon solvation but the latter $\sim$5 kcal/mol.

Since the complete catalytic cycle takes place in heptane,[2,8−10] we estimated $\Delta E_R{}^S{}_{exp}$ with an increasing number of heptane molecules. In the presence of one heptane, molybdenum complexes are similarly affected by the inclusion of solvent ($\Delta\Delta E^S{}_{exp\ (MoN/MoNH+)} \approx \Delta\Delta E^S{}_{exp(MoNNH/MoNNH2+)} \sim 1$ kcal/mol), while $\Delta\Delta E^S{}_{exp\ (Lut/LutH+)}$ is ~ 3 kcal/mol. The addition of a second heptane molecule determines a further increase of both $\Delta\Delta E^S{}_{exp(MoNNH/MoNNH2+)}$ and $\Delta\Delta E^S{}_{exp(Lut/LutH+)}$, whereas $\Delta\Delta E^S{}_{exp(MoN/MoNH+)}$ is hardly changed. The addition of other solvent molecule(s) would render molybdenum species so large that DFT calculations become prohibitive even with considerable computational resources. Thus, solvent corrections for molybdenum species were estimated with two heptane molecules at the most. This is enough to

Table 5. ΔE_R (kcal/mol) of Processes **SIV** and **SVIII**, DFT vs Experimental Results

	in vacuo				in solution						
					C_6H_6			C_7H_{16}			
	BP[a]	BP[b]	B3LYP[c]	BH&H[d]	B3LYP (PCM)[b]	BH&H[b,e]	BH&H[d,e]	B3LYP (PCM)[c]	BH&H[b,e]	BH&H[d,e]	expt (C_6H_6)
SIV	−17.0	−18.9	−18.9	−16.3	−8.7	4.7	2.9	−10.2	−5.3	−4.7	∼0
SVIII	−17.2	−17.8	−15.3	−14.6	−7.9	6.4	4.6	−13.2	−3.6	−3.0	∼ −1

[a] With plane waves. [b] With 6-31+G(d). [c] B3LYP/TZVP ref 25. [d] With BH&H/6-311++G(d,p). [e] Considering solvated $LutH^+$ and Lut with four solvent molecules.

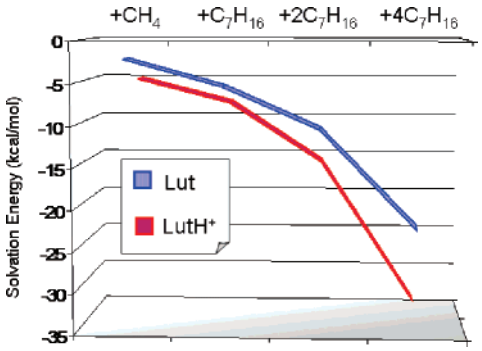

Figure 5. Solvation energies ΔE^S_{exp} vs number of solvent molecules (methane and heptane) for $LutH^+$ (red) and Lut (blue).

provide a rough idea that solvent effects ($\Delta E^S_{exp(MoNNH/MoNNH2+)} < \Delta E^S_{exp(MoN/MoNH+)} < 4$ kcal/mol)[66] are similar for reactants and products and much smaller[67] than that of the proton source. Instead, calculations including four heptane molecules, that virtually represent a first solvation shell, are still affordable for $LutH^+$ and LutH.[68]

As displayed in Table 6 and Figure 5, the solvent effect for the protonation source is quite large, as $\Delta\Delta E^S_{exp(Lut/LutH+)} \sim 11$ kcal/mol. This figure is slightly enhanced if the larger basis set is used (Table 6). Therefore, even an apolar solvent like heptane may play a relevant role for the energetic profile of **SIV** and **SVIII**.[59]

Since measurements of reaction free energies have been carried out in the presence of benzene,[10] this solvent was also taken into account. Considering implicitly benzene solvent reduces $\Delta\Delta E_R{}^S_{PCM}$ to ∼9 and ∼7 kcal/mol for **SIV** and **SVIII**, respectively. Yet, solvent effects are much larger when 2 and 4 benzene molecules are included explicitly in the calculation as $\Delta\Delta E^S_{exp(Lut/LutH+)}$ is ∼ 9 and ∼20 kcal/mol, respectively. Unfortunately, no more than four benzene molecules can be considered as the size of the system becomes rapidly prohibitive even for DFT calculations. Nevertheless, we are confident that four solvent molecules may represent a virtual first solvation shell.[69]

In fact, although the method is highly approximated, several features confirm that a first solvation sphere was achieved for both the benzene and heptane solvation models: (a) solvation energies showed no significant changes when the fourth molecule was added (less than ∼3 kcal/mol); (b) one of the four solvent molecules does not interact directly with the solutes (Figure 6); and (c) four solvent molecules occupy most of the space around both forms of the protonation agent, reducing the probability of a fifth solvent molecule directly interacting with the solutes (Figures 6 and S6). We are, hence, confident that four solvent molecules may represent a good tradeoff between computational costs and the fair description of solvation effects.

Once solvation effects are included in the estimation of reaction energies, discrepancy between experimental free energies and calculated reaction energies is drastically reduced to less than ∼5 kcal/mol for both **SIV** and **SVII** when the large basis set is used (Table 6).[68] Therefore, inclusion of explicit solvent molecules significantly improves the agreement between experimental and calculated reaction energies.

In order to understand the reason why $LutH^+$ undergoes a larger stabilization than Lut in the presence of explicit solvent, the Atoms In Molecules (AIM)[51] analysis was employed (Table 6). In particular, Figure 6 displays a schematic view of C−H...π attractive interactions between four heptane molecules and both $LutH^+$ (Figure 6A′) and Lut (Figure 6B′). Lut(heptane)$_4$ has seven Bond Critical Points (BCPs) corresponding to C−H...π interactions with a total electron density (ρ_{TOT}) equal to 0.0497 au, where $LutH^+$(heptane)$_4$ shows nine BCPs with $\rho_{TOT} = 0.0550$ au. Notably, one of the four heptane molecules in both Lut(heptane)$_4$ and $LutH^+$(heptane)$_4$ is not directly interacting with the solute via attractive interactions. Consistently, π...π interactions are present between benzene molecules and a protonation agent. In particular, for Lut(benzene)$_4$ we observe six BCPs, corresponding to π...π interactions with $\rho_{TOT} = 0.137$ au. On the other hand, $LutH^+$(benzene)$_4$ shows seven BCPs with $\rho_{TOT} = 0.160$ au. Indeed, electron densities reported in Table 6 confirm that $LutH^+$ interacts more strongly with the solvent molecules than Lut. Furthermore, the strength of such interactions depends quite significantly on the solvent employed, providing a rationale for the energies reported in Tables 5 and 6.

In summary, inclusion of explicit apolar solvent molecules sensibly influences the energetic profile of **SIV** and **SVIII**.

Solvation Effect on Reduction Steps. In order to verify whether disagreement between experimental and calculated reaction energies of **SV** and **SIX** may be due to the lack of solvation effects as shown for protonation steps, similar calculations were performed also for the reduction steps. First, reaction energies of **SV** and **SIX** were estimated considering an implicit solvent model. Since experimental energies reported in the literature are measured in PhF,[10] while the reaction actually takes place in heptane, both solvents were considered. With the inclusion of implicit PhF and heptane solvents, the description of reduction steps does not improve. For instance, $\Delta\Delta E_R{}^S_{PCM} \sim 3$ and ∼ 6 kcal/mol

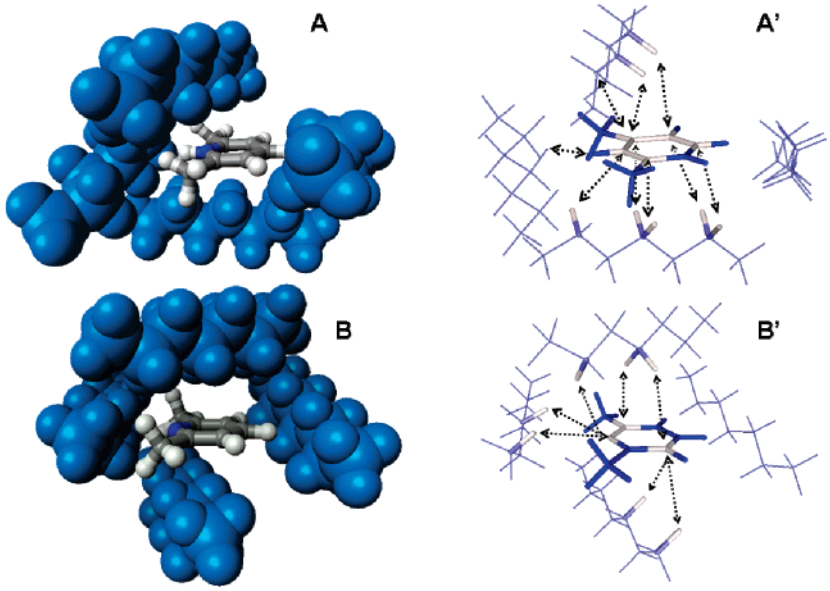

Figure 6. Views of solvation models with four heptane molecules of (A) $LutH^+$ and (B) Lut and schematic view of C−H...π interactions (black arrows) in A′ and B′, respectively.

Table 6. (a) and (b) Solvation Energies (ΔE^S_{exp}) (kcal/mol) and Total Electron Densities (au) of π...π and C−H...π Interactions with Explicit Solvent Molecules

(a)

	+ 1xCH_4		+ 1xC_7H_{16}		+ 2xC_7H_{16}		+ 4xC_7H_{16}		
	ΔE^{Sa}	ρ_{TOT}	ΔE^{Sa}	ρ_{TOT}	ΔE^{Sa}	ρ_{TOT}	ΔE^{Sa}	ρ_{TOT}	+ 4xC_7H_{16} ΔE^{Sb}
Lut	−2.2	0.0081	−5.4	0.0183	−10.5	0.0419	−22.5	0.0497	−25.2
$LutH^+$	−5.1	0.0212	−8.1	0.0300	−15.6	0.0440	−33.5	0.0550	−36.8
MoN	−3.6	0.0160	−2.0	0.0170	−5.8	0.0390			
$MoNH^+$	−3.9	0.0171	−0.6	0.0075	−2.0	0.0320			
MoNNH	−1.7	0.0110	−0.4	0.0200	−0.9	0.0198			
$MoNNH_2^+$	−2.0	0.0140	−1.0	0.0120	−1.9	0.0286			

(b)

	+ 2xC_6H_5F		+ 2xC_7H_{16}		+ 2xC_6H_6		+ 4xC_6H_6		
	ΔE^{Sa}	ρ_{TOT}	ΔE^{Sa}	ρ_{TOT}	ΔE^{Sa}	ρ_{TOT}	ΔE^{Sa}	ρ_{TOT}	+ 4xC_6H_6 ΔE^{Sb}
dmCr	−1.45	0.0212	−2.7	0.0290					
$dmCr^+$	−6.1	0.0510	−4.0	0.0250					
Lut					−7.8	0.0290	−13.2	0.137	−19.8
$LutH^+$					−17.2	0.0890	−34.2	0.160	−39.0

[a] Calculated solvation energies with BHandH/6-31+G(d). [b] Calculated solvation energies with BHandH/6-311++G(d,p).

for **SV** and **SIX** in heptane and $\Delta\Delta E_R{}^S{}_{PCM} \geq 20$ kcal/mol for both reactions in PhF.[35]

Unlike protonation reactions, a correct evaluation of explicit solvation effects for reduction steps present several issues. First, the size of decamethylcromocene is rather large, and calculations of dmCr(heptane)$_n$ complexes become prohibitive already with $n > 2$. Most importantly, the ionization energy of $dmCr^+$/dmCr calculated with BHandH,[20] which is the only exchange-correlation functional among those used in this work that accounts for dispersion interactions,[53] is underestimated (Table 7). Nevertheless, DFT-BHandH[20] calculations were performed to estimate the influence of solvation on the overall reaction energy of reduction steps. As shown in the previous section, solvation effects on reaction intermediates were negligible. Only calculations on $dmCr^+$ and dmCr were carried out by considering two heptane and two PhF molecules explicitly. Interestingly, the effect of heptane solvation is small, for instance $\Delta E^S_{exp}(heptane)_2$ are ~ -3 and ~ -4 kcal/mol for dmCr and $dmCr^+$, respectively (compared with $\Delta E^S_{exp}(heptane)_2 \sim -10$ and ~ -15 kcal/mol of Lut and $LutH^+$). Accordingly, ΔE^S_{exp} $(PhF)_2$ is ~ -1.5 and ~ -6 kcal/mol, for dmCr and $dmCr^+$, respectively, confirming that solvation effects are indeed much smaller than those of the protonation agent (ΔE^S_{exp} $(benzene)_2 \sim -8$ and ~ -17 kcal/mol for Lut and $LutH^+$, respectively). Unlike Lut and $LutH^+$, interactions with heptane are similarly strong for both $dmCr^+$ and dmCr (5 BCPs, $\rho_{TOT} = 0.0290$ and 5 BCPs, $\rho_{TOT} =$

Table 7. Dependence of the Ionization Energy and the ΔE_R for **SV** and **SIX** on the Exchange-Correlation Functionals

		$MoNNH_2^{+/0}$		$MoNH^{+/0}$	
	$dmCr^{+/0}$ IE	IE	ΔE_R(**SV**)	IE	ΔE_R(**SIX**)
expt.[70]	113.7		~ -2		~ -5
B3LYP	100.7	106.5	−5.9	109.0	−8.3
B3LYP[a]	101.6	105.2	−3.6	109.6	−8.0
BLYP	102.5	97.2	5.3	99.6	+2.9
BHandH	89.7	109.9	−20.2	112.0	−22.3
BHandHLYP	89.6	115.6	−26.0	116.7	−27.2
BP	108.5	101.6	6.9	104.0	+4.5
BP[§]	108.5	101.7	6.8	105.5	3.0
B3P	114.4	118.9	−4.5	121.3	−6.9
B3P[§]	114.7	117.4	−2.7	122.2	−7.5
PW91	98.4	107.5	−9.2	110.0	−11.6

[a] Full optimization with localized basis sets, while all other data refer to single point calculations on BP[18,31] optimized geometry with PW basis sets.

0.0250, for dmCr and $dmCr^+$, respectively, Figure S7), resulting in a $\Delta\Delta E^S_{exp}$ $(heptane)_2 \leq 1.5$ kcal/mol. In contrast, two PhF molecules cause a larger difference, yet not significant, between reduced and oxidized dmCr, as $\Delta\Delta E^s_{exp}$ $(PhF)_2 \leq 4.6$ kcal/mol (3 BCPs, $\rho_{TOT} = 0.0212$ and 7 BCPs, $\rho_{TOT} = 0.0510$ for dmCr and $dmCr^+$, respectively). Therefore, no strong solvent effect is expected on the energetics of reduction steps, and in vacuo calculations should provide reasonable reaction energies. Thus, the discrepancy between experimental and calculated reaction energies cannot be solely attributed to the lack of explicit solvent.

Performance of DFT Exchange-Correlation Functionals for Reduction Steps. Since ionization energy (IE) of $dmCr/dmCr^+$ strongly depends on the exchange-correlation functional, its effect on ΔE_R of **SV** and **SIX** was monitored. Ionization energy for $dmCr/dmCr^+$ has been measured as 113.7 kcal/mol.[70] As summarized in Table 7, several DFT functionals provide remarkably discrepant results (ranging between 89 and 114 kcal/mol). IEs were evaluated either minimizing the structure or performing SP calculations on the BP[18,31] optimized structures.[71]

Among all functionals, B3P[20,31] and BP[18,31] give the best agreement with experimental IE,[70] while those estimated with BHandH[20] and BHandLYP[20,19] are strongly underestimated.

Similarly, IEs of the catalytic intermediates redox couples largely depend on the DFT functionals, with IE($MoNH^+$/MoNH) and IE($MoNNH_2^+$/$MoNNH_2$) ranging between ~97/~117 kcal/mol and ~99/~122, respectively. As a consequence, calculated ΔE_R(**SV**) and ΔE_R(**SIX**) range between −26.0/+6.9 kcal/mol and −27.2 /+4.5 kcal/mol. Thus, reduction steps $\Delta\Delta E_R$ is mainly affected by the errors in the estimation of the ionization energies.

Our results indicate that DFT functionals B3LYP[19,20] and B3P[20,31] are the only ones able of reproducing **SIV** and **SVIII** reaction energies within an error of 2−3 kcal/mol. However, the correct value produced by B3LYP[20,19] is likely due to a fortuitous cancellation of error, as IE($dmCr/dmCr^+$) calculated with B3LYP was quite different from the experimental data (ΔIE ~ 12 kcal/mol). Thus, B3P[20,31] is the only exchange-correlation functional reproducing both IE and ΔE_R correctly.

Conclusions

We performed a structural and electronic characterization of Mo($HIPTN_3N$) (with HIPT = hexaisopropylterphenyl) a compound that performs the same catalytic function of the enzyme nitrogenase.[2,8] Our calculations suggest that the chelating ligand rigidity is mainly responsible for the structural properties of the catalyst. In agreement with experimental findings,[2,8−10] we showed that the large HIPT substituents hardly affect the structural and electronic properties of the catalyst, playing only a steric role that hampers formation of catalyst dimers.[8−10] At the same time, the bulky HIPT substituents create a cage in which the molecular nitrogen binds in an end-on-fashion.

Using a relatively small computational model (**B**, Figure 1), which reproduces the structural and electronic properties of the full complex (**A**, Figure 1), we described the electronic and structural features of possible catalytic intermediates of the Chatt-like mechanism in Figure 2. A visual inspection of the Kohn−Sham orbitals reveals that the HOMO orbital represents a π^*-back-donation from the filled d_{xz} metal orbital to the empty π^* orbital of N_2[28,54] This orbital is common to all reaction intermediates **I**−**V** suggesting the back-donation as the electronic mechanism responsible for the activation of N_2.

An increase of the N_1-N_2 bond lengths (with a concomitant decrease of the bond order) is observed for the first half reaction, while $Mo-N_1$ bond lengths do not follow any trend because of the combination of steric and electronic effects that come along with the change in hybridization of both nitrogen atoms. In contrast, the $Mo-N_1$ bond constantly decreases in the second half of the catalytic cycle.

Notably, calculated reaction energies are remarkably different from experimental ones even considering implicit solvent models.[25] However, ΔE_R, corrected by taking into account explicit solvent molecules around the protonation agent, reduces the discrepancy for protonation steps to less than roughly 5 kcal/mol. Thus, a lack of explicit solvent may be one of the reasons of the observed discrepancy for protonation steps.[59]

In contrast, an explicit solvation does not improve the agreement for reduction steps, where the discrepancy is mainly associated with the dependence of the ionization energies on the DFT exchange-correlation functionals.

In conclusion, our results show that DFT calculations are a powerful tool to unveil structural and electronic properties of the intermediates of the catalytic cycle. However, due to the complexity of the catalytic system, reaction energies cannot be easily reproduced, limiting the predictability of such calculations.

Acknowledgment. We thank the CINECA computing center, Bologna, Italy and the CNR-INFM grants for the computational resources. Financial support has been provided by the MURST grant 'Fondo per il sostegno dei giovani e per favorire la mobilita' degli studenti'.

Supporting Information Available: Test calculations on the dependence of the geometries on the basis sets and the exchange-correlation functionals and figures illustrating the electronic structure and the solvation model employed. This material is available free of charge via the Internet at http://pubs.acs.org.

References

(1) Modak, J. M. *Resonance* **2002**, 69.

(2) Schrock, R. R. *Acc. Chem. Res.* **2005**, *38*, 955−962.

(3) Schrock, R. R. *Proc. Natl. Acad. Sci. U.S.A.* **2006**, *103*, 17087−17087.

(4) Howard, J. B.; Rees, D. C. *Proc. Natl. Acad. Sci. U.S.A.* **2006**, 1*03*, 17088−17093.

(5) Rees, D. C.; Howard, J. B. *Curr. Opin. Chem. Biol.* **2000**, *4*, 559−566, and references therein.

(6) Burgess, B. K. *Chem. Rev.* **1990**, *90*, 1377−1406.

(7) Burgess, K. B.; Lowe, D. J. *Chem. Rev.* **1996**, *96*, 2983−3011.

(8) Yandulov, D. V.; Schrock, R. R *Science* **2003**, *301*, 76−78.

(9) Yandulov, D. V.; Schrock, R. R.; Rheingold, A. L.; Ceccarelli, C.; Davis, W. M. *Inorg. Chem.* **2003**, *42*, 796−813.

(10) Yandulov, D. V.; Schrock, R. R. *Inorg. Chem.* **2005**, *44*, 1103−1117.

(11) Mackay, B. A.; Fryzuk, M. D. *Chem. Rev.* **2004**, *104*, 385−401.

(12) Pickett, C. J. *J. Biol. Inorg. Chem.* **1996**, *1*, 601−606.

(13) Chatt, J.; Dilworth, J. R.; Richards, R. L. *Chem. Rev.* **1978**, *78*, 589−625.

(14) Weare, W. W.; Dai, X.; Brynes, M. J.; Chin, J. M.; Schrock, R. R. Mueller, P. *Proc. Natl. Acad. Sci. U.S.A.* **2006**, *103*, 17099−17106.

(15) Smythe, N. C.; Schrock, R. R, Muller, P.; Weare, W. W. *Inorg. Chem.* **2006**, 45, 9197−9205.

(16) Smythe, N. C.; Schrock, R. R.; Muller, P.; Weare, W. W. *Inorg. Chem.* **2006**, *45*, 7111−7118.

(17) (a) Ritleng, V.; Yandulov, D. V.; Weare, W. W.; Schrock, R. R.; Hock, A. S.; Davis, W. M. *J. Am. Chem. Soc.* **2004**, *126*, 6150−6163. (b) Weare, W. W.; Schrock, R. R.; Hock, A. S.; Muller, P. *Inorg. Chem.* **2006**, *45*, 9185−9196.

(18) Becke, A. D. *Phys. Rev. A* **1988**, *38*, 3098−3100.

(19) Lee, C. T.; Yang, W. T.; Parr, R. G. *Phys. Rev. B* **1988**, 37, 785−789.

(20) (a) Becke, A. D. *J. Chem. Phys.* **1993**, 98, 5648−5652. (b) Becke; A. D. *J. Chem. Phys.* **1993** *98*, 1372−1377.

(21) Cammi, R.; Mennucci, B.; Tomasi, J. *J. Phys. Chem. A* **2000**, *103*, 9100- 9108.

(22) (a) Mo, S. J.; Vreven, T.; Mennucci, B.; Morokuma, K.; Tomasi, J. *Theor. Chem. Acc.* **2004**, *111*, 154−161. (b) Balcells, D.; Carbo, J. J.; Maseras, F.; Eisenstein, O. *Organometallics* **2004**, *23*, 6008−6014. (c) Belkova, N. V.; Besora, M.; Epstein, L. M.; Lledos, A.; Maseras, F.; Shubina, E. S. *J. Am. Chem. Soc.* **2003**, *125*, 7715−7725. (d) De Abreu, H. A.; Guimaraes, L.; Duarte, H. A. *J. Phys. Chem. A* **2006**, *110*, 7713−7718. (e) Kovacs, G.; Papai, I. *Organometallics* **2006**, *25*, 820−825. (f) Begue, D.; Carbonniere, P.; Barone, V.; Pouchan, C. *Chem. Phys. Lett.* **2005**, *416*, 206−211.

(23) Zexing, C.; Zhou, Z.; Wan, H.; Zhang, Q. *Int. J. Quantum Chem.* **2005**, 103, 344−353.

(24) Neese, F. *Angew. Chem., Int. Ed.* **2006**, *45*, 196−199.

(25) Studt, F.; Tuczek, F. *Angew. Chem., Int. Ed.* **2005**, *44*, 5639−5642.

(26) Studt, F.; Tuczek, F. *J. Comput. Chem.* **2006**, *27*, 1278−1291.

(27) Reiher, M.; Le Guennic, B.; Kirchner, B. *Inorg. Chem.* **2005**, *44*, 9640−9642.

(28) Le Guennic, B.; Kirchner, B.; Reiher, M. *Chem. Eur. J.* **2005**, *11*, 7448−7460.

(29) Hölscher M.; Leitner, W. *Eur. J. Inorg. Chem.* **2006**, 4407−4417.

(30) Carr, R.; Parrinello, M. *Phys. Rev. Lett.* **1985**, *55*, 2471.

(31) Perdew, J. P. *Phys. Rev. B* **1986**, *33*, 8822−8824.

(32) (a) Magistrato, A.; Woo, T. K.; Togni, A.; Rothlisberger, U. *Organometallics* **2004**, *23*, 3218−3227. (b) Magistrato, A.; Togni, A.; Rothlisberger, U. *Organometallics* **2006**, *25*, 1151−1157.

(33) Maurer, P.; Magistrato, A.; Rothlisberger, U. *J. Phys. Chem. A* **2004**, *108*, 11494−11499.

(34) Perdew, J. P.; Wang, Y. *Phys. Rev. B* **1986**, *33*, 8800−8802.

(35) PhCl has been considered for PCM calculations since PhF is not available in the Gaussian03 package.

(36) We have to remark that our calculated ΔE do not account for entropic effects.

(37) Baerends, E. J.; Ellis, D. E.; Ros, P. *Chem. Phys.* **1973**, *2*, 41−51.

(38) Baerends, E. J.; Ros, P. *Chem. Phys.* **1973**, *2*, 52−59.

(39) (a) van Lenthe, E.; Ehlers, A. E.; Baerends, E. J. *J. Chem. Phys.* **1999**, *110*, 8943−8953. (b)van Lenthe, E.; Baerends, E. J. Snijders J. G. *J. Chem. Phys.* **1993**, *99*, 4597−4610.

(40) Hutter, J.; Ballone, P.; Bernasconi, M.; Focher, P.; Fois, E.; Goedecker, S.; Parrinello, M.; Tuckerman, M. Max-Planck-Institut für Festkörperforschung and IBM Zurich Research Laboratory, 1995−1996.

(41) (a) Goedecker, S.; Teter, M.; Hutter, J. *Phys. Rev. B* **1996**, *54*, 1703−1710. (b) Hartwigsen, C.; Goedecker, S.; Hutter, J. *Phys. Rev. B* **1998**, *58*, 3641−3662.

(42) Trouillier, N.; Martins, J. L. *Phys. Rev. B* **1991**, *43*, 1993−2006.

(43) Kleinman, L.; Bylander, D. M. *Phys. Rev. Lett.* **1982**, *48*, 1425−1428.

(44) Hockney, R. W. *Methods Comput. Phys.* **1970**, *9*, 136−211. (b) Barnett, R. N.; Landmann, U. *Phys. Rev. B* **1993**, *48*, 2081−2097.

(45) Frisch, M. J. T.; G. W.; Schlegel, H. B.; Scuseria, G. E.; Robb, M. A.; Cheeseman, J. R.; Montgomery, J. A., Jr.; Vreven, T.; Kudin, K. N.; Burant, J. C.; Millam, J. M.; Iyengar, S. S.; Tomasi, J.; Barone, V.; Mennucci, B.; Cossi, M.; Scalmani, G.; Rega, N.; Petersson, G. A.; Nakatsuji, H.; Hada, M.; Ehara, M.; Toyota, K.; Fukuda, R.; Hasegawa, J.; Ishida, M.; Nakajima, T.; Honda, Y.; Kitao, O.; Nakai, H.; Klene, M.; Li, X.; Knox, J. E.; Hratchian, H. P.; Cross, J. B.; Adamo, C.; Jaramillo, J.; Gomperts, R.; Stratmann, R. E.; Yazyev, O.; Austin, A. J.; Cammi, R.; Pomelli, C.; Ochterski, J. W.; Ayala, P. Y.; Morokuma, K.; Voth, G. A.; Salvador, P.; Dannenberg, J. J.; Zakrzewski, V. G.; Dapprich,

S.; Daniels, A. D.; Strain, M. C.; Farkas, O.; Malick, D. K.; Rabuck, A. D.; Raghavachari, K.; Foresman, J. B.; Ortiz, J. V.; Cui, Q.; Baboul, A. G.; Clifford, S.; Cioslowski, J.; Stefanov, B. B.; Liu, G.; Liashenko, A.; Piskorz, P.; Komaromi, I.; Martin, R. L.; Fox, D. J.; Keith, T.; Al-Laham, M. A.; Peng, C. Y.; Nanayakkara, A.; Challacombe, M.; Gill, P. M. W.; Johnson, B.; Chen, W.; Wong, M. W.; Gonzalez, C.; Pople, J. A. Gaussian, Inc.: Pittsburgh, PA, 2003.

(46) Magistrato, A.; Maurer, P.; Fassler, T.; Rothlisherger, U. *J. Phys. Chem. A* **2004**, *108*, 2008−2013.

(47) Marzari, N.; Vanderbilt, D. *Phys. Rev. B* **1997**, *56*, 12847−12856.

(48) Alber, F.; Folkers, G.; Carloni, P. *J. Phys. Chem. B* **1999**, *103*, 6121−6126.

(49) Bader, R. F. W. *Chem. Rev.* **1991**, *91*, 893−928.

(50) Bader, R. F. W. *Atoms in Molecules-A Quantum Theory*; Oxford, University Press: Oxford, 1990.

(51) Bieglerkonig, F. W.; Bader, R. F. W.; Tang, T. H. *J. Comput. Chem.* **1982**, *3*, 317−328.

(52) Bader, R. F. W.; Essen, H. *J. Chem. Phys.* **1984**, *80*, 1943−1960.

(53) Waller, M. P.; Robertazzi, A.; Platts, J. A.; Hibbs, D. E.; Williams, P. A. *J. Comput. Chem.* **2006**, *27*, 491−504.

(54) (a) Cui, Q.; Musaev, D. G.; Svensson, M.; Sieber, S.; Morokuma, K. *J. Am. Chem. Soc.* **1997**, *117*, 12366−12367. (b) Khoroshun, D. V.; Musaev, D. G.; Morokuma, K. *Mol. Phys.* **2002**, *100*, 523−532.

(55) Cotton, F. A.; Wilkinson, G. *Advanced Inorganic Chemistry*; John Wiley and Sons Inc.: New York, 1980.

(56) It has not been possible to localize an energy barrier for this reaction step.

(57) It is likely that, in the presence of the large HIPT substituents, these steric effects are further enhanced.

(58) Friesner, R. A. *Proc. Natl. Acad. Sci. U.S.A.* **2005**, *102*, 6648−6653.

(59) Also the effect of the counterions, totally neglected in our calculation, may have an important role for the reaction energies.

(60) (a) Ye, X. Y.; Li, Z. H.; Wang, W. N.; Fan, K. N.; Xu, W.; Hua, Z. Y. *Chem. Phys. Lett.* **2004**, *397*, 56−61. (b) Johnson, E. R.; Wolkow, R. A.; DiLabio, G. A. *Chem. Phys. Lett.* **2004**, *394*, 334−338. (c) VandeVondele, J.; Lynden-Bell, R.; Meijer, E. J.; Sprik, M. *J. Phys. Chem. B* **2006**, *110*, 3614−3623.

(61) Head-Gordon, M.; Pople, J. A.; Frisch, M. J. *Chem. Phys. Lett.* **1988**, *153*, 503.

(62) (a) Cizek, J. *Adv. Chem. Phys.* **1969**, *14*, 35. (b) Hobza, P.; Sponer, J. *J. Am. Chem. Soc.* **2002**, *124*, 11802−11808. (c) Jurecka, P.; Hobza, P. *J. Am. Chem. Soc.* **2003**, *125*, 15608−15613.

(63) (a) Robertazzi, A.; Platts, J. A. *J. Phys. Chem. A* **2006**, *110*, (11), 3992−4000. (b) Robertazzi, A.; Platts, J. A. *Chem. Eur. J.* **2006**, *12*, 5747−5756.

(64) Burda, J.; Sokalski, A.; Leszczynski, J. *J. Mol. Model.* **2007**, *13*, 335−345.

(65) Shibasaki, K.; Fujii, A.; Mikami, N.; Tsuzuki, S. *J. Phys. Chem. A* **2006**, *110*, 4397−4404.

(66) The effect of explicit solvation on reaction intermediates is not considered since it is similar for neutral and positively charged reaction intermediates, thus it is expected not to significantly improve the calculation of reaction energies.

(67) Molybdenum complexes employed in experiments are larger than the model used, and the metal center is less accessible to solvent molecules. Thus, the effects of solvent may be even smaller than those obtained in this work.

(68) Solvation energies of Lut and $LutH^+$ estimated with three and four heptane molecules are very similar (data not shown), suggesting that adding more solvent molecules would not largely affect solvation energies. Thus, four heptane molecules may constitute the first solvation shell.

(69) Firstly, four benzene molecules occupy the entire space around the solute; therefore, a further solvent molecule would interact with one of the benzenes rather than with the solute. Secondly, solvation energies estimated with three and four benzenes are very similar (data not shown).

(70) Ryan, M. F.; Richardson, D. E.; Lichtenberger, D. L.; Gruhn, N. E. *Organometallics* **1994**, *13*, 1190−1199.

(71) A rough idea of exchange-correlation influence is estimated also by performing SP calculations on the $BP^{18,31}$ optimized geometries. Indeed, performing SP calculations on the $BP^{18,31}$ optimized geometry with a different functional we observe a maximal error of $\Delta E \sim 1.5$ kcal/mol, with respect to the total energy we would obtain relaxing geometry with the functional chosen.

CT700094Y